An ultrastable platform for the study of single-atom chains

D. T. Smith,[a)] J. R. Pratt, F. Tavazza, L. E. Levine, and A. M. Chaka
National Institute of Standards and Technology, Gaithersburg, Maryland 20899, USA

We describe a surface probe instrument capable of sustaining single atomic bond junctions in the electronic quantum conduction regime for tens of minutes, and present results for Au junctions that can be "locked" stably in $n=1$ and $n=2$ quantum conduction states with electrical conductivity nG_0 ($G_0=2e^2/h$) and switched in a controlled way. The instrument measures and controls the gap formed between a probe and a flat surface with better than 5 pm long-term stability in a high-vacuum chamber at 4 K using a high-sensitivity fiber-optic interferometer that forms a Fabry–Perot cavity immediately adjacent and parallel to the probe. We also report the experimental observation of stable noninteger conduction states, along with preliminary density functional theory-based calculations of one-dimensional (1D) and two-dimensional Au "bridges" that produce comparable noninteger conduction states. Finally, we report the observation of novel stochastic processes related to nonballistic electron transport through strained single atomic bond junctions. The instrument permits detailed study of electron transport in 1D systems, and the long-term picometer stability of the junction holds great promise for application to single-molecule spectroscopy. © *2010 American Institute of Physics*. [doi:10.1063/1.3369584]

I. INTRODUCTION

The study of the mechanical and transport properties of atomic-size contacts is a very active area of research (see Ref. 1 for a comprehensive review). These studies present a rare opportunity to make quantitative comparisons between theory and experiment regarding atomic interaction potentials and quantum effects such as shot noise and Coulomb blockades, while providing access to the complex interplay of mechanical, electrical, and chemical properties that occur only at this scale.

We have developed an experimental platform, which we refer to as a feedback-stabilized break junction (FSBJ), to create and deform stable atomic-scale contacts, and have used that platform to probe the phenomenon of quantized electrical conductance in Au nanowires and single-atom chains (SACs). In such a system, electrical conductivity, σ, is known to be quantized in units of $G_0=2e^2/h$; that is, $\sigma=nG_0$ for integer n, with e the charge of the electron and h Plank's constant.[2–4] The conductivity for the $n=1$ state corresponds to a contact resistance of 12.9 kΩ. Quantized conductance has been observed many times, but experimental instabilities typically limit the time a given contact stays in a low-n state to milliseconds,[5] and often the presence of quantized states must be inferred from histograms compiled from hundreds or thousands of junction breaks.[1,6] Because the $n=1$ conduction state is believed to occur when there is only one electron conduction channel through the contact,[7,8] the ability to maintain that state indefinitely would clearly demonstrate exceptional experimental stability.

Two types of measurement platforms have been employed in most studies of atomic-size contacts. These are mechanically controlled break junctions (MCBJs) (Refs. 9–11) and scanning probe microscopes (SPMs).[12,13] MCBJs are typically formed by stretching a small electrically conducting wire[9,11] or thin film[10] mounted on a substrate at 4 K, with strain at the junction controlled stably by a piezoelectric actuator that bends the substrate. The chief advantage of the MCBJ is its remarkable mechanical stability (<1 pm/h drift of the electrodes has been demonstrated at cryogenic temperatures[14]). Some MCBJ experiments have also included a tuning fork force sensor to measure contact stiffness.[15,16] The chief difficulty with MCBJs is that the calibration of the electrode separation is typically inferred through reference to Gundlach oscillations,[17] also known as "field emission resonances," which are thought to provide a length scale that is accurate to only 20%,[18] and which have never been compared directly to an absolute length standard. Also, if the junction fails, for example due to the presence of a contaminant atom or molecule, the MCBJ technique does not allow an *in situ* movement to a new contact location; the experiment must be warmed to room temperature and the junction replaced.

Atomic-scale electrical junctions have also been investigated using SPMs with electrically conductive tips, with scanning tunneling microscopes (STMs) particularly well-suited to such studies.[13] Scanning provides the ability to image the electrode surface,[19] and the flexibility to form junctions at various locations on the flat surface without a return to room temperature. Junctions are formed by "crashing" the probe into a flat surface, allowing the probe and surface to weld, then drawing a nanowire from the contact. The advantages of this approach are rapid experimentation and the ability to calibrate the probe displacement by scanning over nanometer-scale step height standards. Some STM experiments have also been performed with the flat surface located on a force-sensing cantilever, enabling simultaneous measurement of current through the junction and the mechanical

---

a)Author to whom correspondence should be addressed. Electronic mail: douglas.smith@nist.gov.

force across the junction.[19–23] The disadvantage to SPM-based methods is that positional stability is substantially reduced compared to that of a MCBJ, and can only be obtained through extensive vibration isolation, although in recent work interferometer feedback has been used to counteract vibrations in the frame of a commercial SPM.[24]

In addition, there have also been experiments in which nanoscale junctions are formed and broken within a transmission electron microscope.[5,25–27] These experiments provide intriguing real-time images of nanowires and SACs as they are drawn and broken, but operation in the room temperature, relatively low-vacuum environment of an electron microscope generally prohibits the detailed study of SACs that are stable for seconds or minutes.

Atomic-scale junctions have also proven fertile ground for theoretical investigations, primarily due to their often unique physical, chemical, and electrical properties. Research into Au nanowires has been particularly fruitful, as this ductile metal can thin down to SACs, allowing detailed studies of the relationship between atomic structure and quantum electron transport behavior.[5,28–31] For example, a recent study by three of the present authors used semistatic density functional theory (DFT) to explore the evolution of [110] and [111] Au nanowires during tensile deformation under a wide range of tensile axes (along high- and low-symmetry directions), nanowire shapes, and effective strain rates. A rich diversity of deformation pathways was uncovered, and four stable intermediate atomic configurations were identified. The abrupt transitions between conductive states observed experimentally in this work likely correspond to progressive morphological transitions between these intermediate configurations and SACs. Quantum-mechanics-based simulations of electron transport in these structures are thus necessary to "close the loop" between experiment and theory and provide an experimentally validated description of both the structural evolution and conductance behavior of deforming Au nanowires.

II. EXPERIMENTAL DESIGN

A. Break junction mechanical design

The FSBJ instrument we present here provides high stability and an unprecedented accuracy in displacement measurement for the study of atomic point contacts by combining the displacement measurement and positioning capabilities of STM with the exceptional stability of a MCBJ system. It is essentially an STM equipped with an ultrastable, high-resolution homodyne optical-fiber interferometer that forms a Fabry–Perot (FP) cavity immediately adjacent to the probe, as shown in Fig. 1(a). An opposing Au flat serves as both the counter-electrode for the Au probe tip and the reflecting surface for the FP cavity. By using feedback from the interferometer to "lock" the cavity length, we create a platform that gives us the long-term stability of the best cryo-STM systems, at a fraction of the cost, and the feedback allows us to maintain that stable position control even when sweeping temperature or magnetic field, processes that would seriously degrade the stability of open-loop systems.
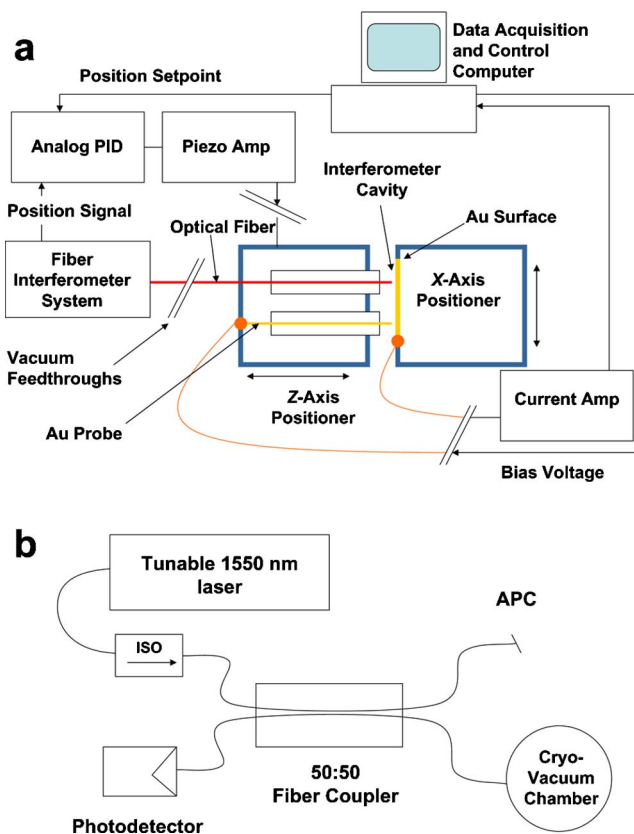

FIG. 1. (Color online) (a) A schematic of the FSBJ experimental system, consisting of a gold probe and flat, optical fiber, and the *z*-axis and *x*-axis positioners inside the cryovacuum chamber as well as external electronic instrumentation related to the positional feedback control loop. An FP cavity is formed between the cleaved end of the optical fiber and the flat Au surface; the cavity is approximately 50 μm long when the Au tip touches the Au surface. (b) Schematic diagram of that part of the fiber-optic interferometer system external to the cryovacuum chamber and consisting of the tunable IR laser, an optical isolator, evanescent wave coupler, angle-polished connector, and single cavity photodetector.

Positioning of the probe and optical fiber assembly relative to the Au flat is accomplished with two piezoelectric nanopositioners[32] capable of both linear step motion over 3 mm or more and fine piezoelectric extension with subpicometer control in vacuum at 4 K. One positioner moves the plate supporting the probe and optical fiber toward and away from the Au flat [the "*z*-axis" direction in Fig. 1(a)]. The second positioner moves the Au flat perpendicular to the *z*-axis [the "*x*-axis" in Fig. 1(a)], allowing us to move to new positions on the Au flat as needed. The entire assembly is mounted to a base plate at the center of an inexpensive commercial cryogenic vacuum probe station chamber that allows stable operation at 4 K, providing what is effectively an ultrahigh-vacuum (UHV) environment for the experiments. We cannot, however, prepare our tips and surfaces under UHV. Adsorption of gases on the probe and flat during cooldown is avoided by cooling the radiation shields surrounding the experimental assembly to 4 K before cooling the assembly, but we certainly have adsorbed contaminants on both our tip and flat surface after cooling to 4 K. We mitigate the effects of this layer by "working" the Au junction; we repeatedly make and break contacts until we are able to draw a SAC with $n \approx 1$ conductance. Although we cannot change

the tip *in situ*, we sometimes find that a persistent contamination problem can be "fixed" by moving the Au flat laterally so that the tip contacts a new location.

We form our Au probes by simultaneously heating and drawing 100 μm diameter Au wire (99.99% purity) until it separates when a necked section melts. The probe and the optical fiber are supported by parallel glass ferrules with 1.8 mm outside diameter and a 125 μm inner bore, which matches the diameter of the optical fiber. The Au probe tip and optical fiber end are positioned relative to each other in the z direction such that when the probe tip just touches the flat, a FP cavity approximately 50 μm long is formed between the cleaved fiber end and the Au flat. In this configuration, the interferometer directly measures the motion of the probe tip relative to the Au flat. This motion corresponds closely to nanowire elongation prior to rupture when a junction is present, or the electrode separation after rupture, but we recognize that there may be small tensile strains in the "grips" when a nanowire is present, or across the gap when the chain is "broken" but very close to contact; such strains would not allow us to say with certainty that the motion of the macroscopic tip is identical to nanowire elongation or change in gap length to within the picometer accuracy that we measure it. This tensile strain effect at atomic point contacts has been studied in some detail by Trouwborst *et al.*[33]

Wires are connected to both the probe and flat, a bias voltage of 5.0 mV dc is applied across the contact and current through the contact is measured with a commercial transimpedance amplifier. For a 5.0 mV bias voltage, one conductance quantum $G_0 = 2e^2/h$ corresponds to a current of 390 nA.

B. Fiber-optic FP interferometer

The basic design of the fiber-optic interferometer is shown in Fig. 1(b). Details of the interferometer construction and performance are described elsewhere,[34] but it is essentially a homodyne FP system with a wavelength-tunable infrared (IR) laser source and a single photodetector. When the cavity length is swept continuously over multiple wavelengths of the laser source (nominal laser wavelength $\lambda = 1550$ nm), the intensity of the IR signal measured by the photodetector varies sinusoidally with consecutive maxima formed by constructive interference (or minima from destructive interference) of reflections from the cleaved fiber end and the Au flat occurring each time the cavity length changes by $\lambda/2$. Laser output power (typically 0.3 to 0.5 mW) and electronic gain in the system are adjusted such that the detection system outputs 10 V at constructive maxima. Destructive minima have values around 1 V; the minima are not zero because the reflectivity of the Au surface is greater than that of the glass/vacuum interface at the cleaved fiber end, and the FP cavity is not symmetric. The interferometer is most sensitive for combinations of wavelength and cavity length that place the detector output at an inflection (or quadrature) point on the sine wave (at or near 5.5 V), where the greatest change in output voltage occurs for a given change in cavity length. In this work, typical interferometer sensitivity was 40 mV/nm. Because the operating cavity
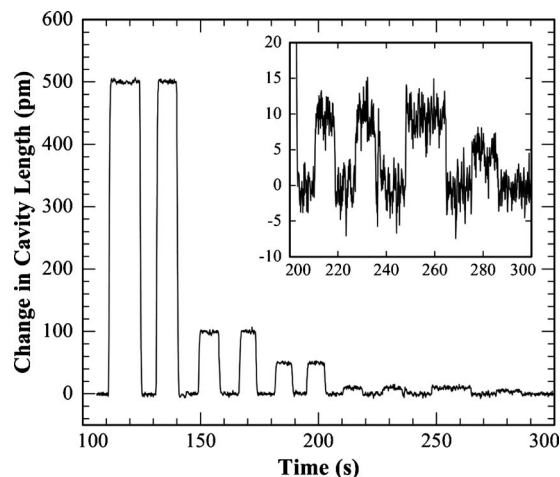

FIG. 2. Observed changes in the interferometer cavity length as the servo set point is changed. The inset is a magnification of the data from 200 to 300 s. Set point changes were 500, 100, 50, 10, and 5 pm; changes as small as 5 pm produced well-defined changes in the cavity length. The data were taken in vacuum at 4 K.

length was typically determined by the Au–Au junction formed, the interferometer was "tuned" to quadrature by adjusting the laser wavelength when an Au junction was formed. For FP cavity lengths of the order of 50 μm between a cleaved glass fiber and a highly reflecting Au surface, we have determined that the interferometer resolution is noise-limited at 2 pm for quasistatic cavity measurements and at approximately 40 fm when sinusoidal position modulation (at 10 Hz or greater) is employed.[34]

The FSBJ can actively maintain a constant separation between the Au surface and the fiber end, and therefore the probe tip, by using the interferometer output to control the z-axis positioner. The bandwidth of the control loop is limited by the positioner dynamics to approximately 200 Hz, but this is sufficient for the cancellation of drift and low-frequency seismic and air-handling vibrations. When changing the position set point in the control loop, cavity length changes as small as 5 pm can be clearly resolved; Fig. 2 shows measured changes in cavity length resulting from set point changes. These length changes may be made traceable to the international system of units through laser wavelength calibration.[35]

C. Interferometer stability cross-check

The simple observance of a stable output from the interferometer system when under servo control does not prove that the cavity length is in fact being held constant, as any drift or instability elsewhere in the interferometer system—in the fiber itself or the detection electronics—will become part of the feedback signal, and the interferometer output will appear stable even if the cavity length is not. In Sec. III, we show that we are able to maintain SACs in specific quantized conduction states essentially indefinitely when the probe position is under interferometer servo control; this ability provides strong indirect evidence that the probe tip is being held in place with subnanometer stability.

However, we have been able to make a more quantitative assessment of interferometer stability by constructing a sec-
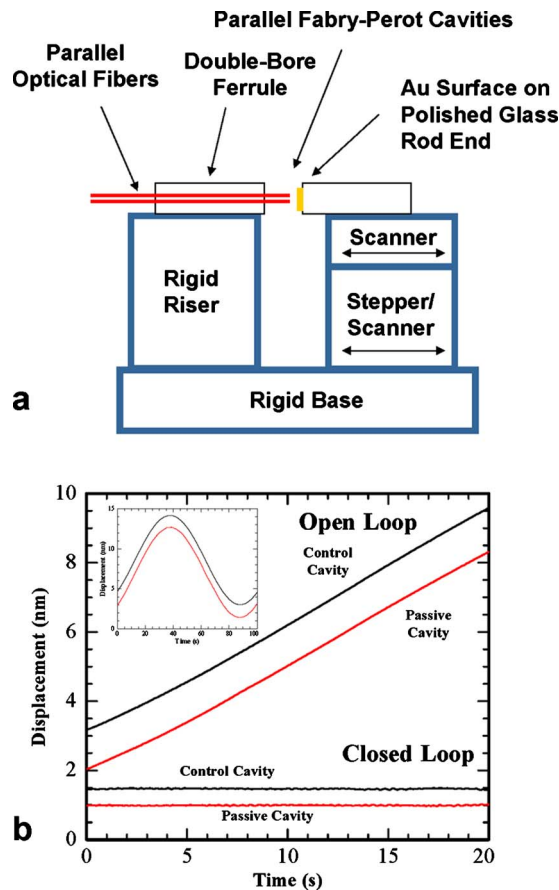
FIG. 3. (Color online) (a) Schematic diagram of the experimental arrangement used to check for drift in the interferometer system. Two entirely independent interferometers [as shown in Fig. 1(a)] were constructed, with the cleaved ends on parallel fibers forming cavities with a common Au surface. (b) A 0.01 Hz, 11 nm peak-to-peak sine wave drive (inset) was applied to the "stepper/scanner" stage to simulate slow, common-mode drift of the cavity lengths. The main figure in (b) shows the response of both interferometers with no feedback (open loop) and with the output from the control interferometer (upper traces, in black) used to lock the cavity length (closed loop) using an applied voltage to the upper scanner while maintaining the sine wave drive to the lower scanner. The data were taken in air at room temperature.

ond, completely independent interferometer system, and operating it in parallel with the first, using the reflecting Au flat as the common reflecting surface for both FP cavities, as shown in Fig. 3(a). Except for the Au flat, all other components—lasers, isolators, couplers, detectors, and current amplifiers—are separate for the two systems. This dual-interferometer cross-check was relatively simple for us, as we had already built a complete second interferometer for another purpose. The basis of the stability test was to use one interferometer output signal to lock the cavity length and then observe any changes in the output of the other interferometer. Because the arrangement shown in Fig. 3(a) is not the standard vacuum-cryogenic experimental configuration, this stability cross-check was performed in air at room temperature. The double cavity could have been moved into the cryovacuum environment without a great deal of trouble, had that proven necessary, but we found the results in air reported below to be perfectly satisfactory for confirming interferometer stability.

The results of the cross-check are shown in Fig. 3(b). Even though the experimental assembly was operated in air at room temperature, typical drift rates were too low to provide a rigorous test of stability under servo control (although they would have been too large to permit SAC studies without feedback, had we been attempting that). Therefore, an artificial "drift" in cavity length was introduced by driving the lower stepper/scanner positioner supporting the Au surface with a 0.01 Hz sine wave at an amplitude that produced an 11 nm peak-to-peak motion of the Au flat relative to the ends of the optical fibers when the servo control was turned off. The output of both interferometers near an inflection point of the sine wave drive, where the effective drift rate is greatest, is shown as the "open loop" traces in Fig. 3(b) (a full 100 s cycle of the sine wave drive is shown in the inset). The output signals from the two interferometers are seen to track each other closely. The servo loop is then closed by using the output of one interferometer (termed the "control cavity") to drive the upper scanner under the Au flat such that the length of the control cavity is locked, while maintaining the 0.01 Hz, 11 nm drive to the lower scanner. The interferometer outputs for both the "control" and "passive" cavities under these conditions are shown in the traces labeled "closed loop."

Cavity length measurements made under these ambient conditions are, not surprisingly, somewhat noisier than those under vacuum at 4 K; approximately 20 pm rms noise is observed for both cavities under both open-loop and closed-loop operating conditions and can clearly be seen on the closed-loop traces. However, the long-term drift observed in the passive cavity under closed-loop conditions was observed to be less than 0.25 pm s^{-1} over hundreds of seconds, a stability comparable to that seen in the output of the control cavity. Because the only common component between the two systems is the Au flat, the fact that the output for the passive interferometer is seen to be as stable as the output of the control system clearly demonstrates that each interferometer system is stable at the picometer level.

III. RESULTS

When using the FSBJ to study the formation, elongation, and rupture of Au nanowires and SACs, we observe a wide range of electrical conduction behavior. In Fig. 4, we show typical results for the conductance that we observe, in units of $G_0 = 2e^2/h$, as the probe tip is moved relative to the flat. The data were taken with the junction under vacuum at 4 K, by first making and breaking a contact several times, then making a contact and drawing it out to the $n=1$ conduction state by slowly changing the position set point. The data begin (at time $t \equiv 0$ s) with the system stable in the $n=1$ state. Over the time shown, we broke the contact, remade it, and broke it again. In addition to conduction at, or very near, integer conduction states, the data also show stable conduction states at noninteger values. Conduction states at $n=1$ and 2 were quite reproducible from contact to contact, but we also observed a variety of stable noninteger conduction states, some of which are visible in Fig. 4; they will be discussed below. Under feedback control, we were routinely
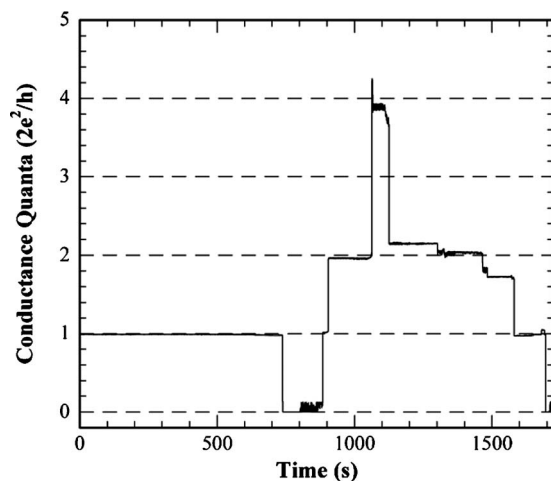
FIG. 4. Electrical conductance through a Au–Au atomic point contact in vacuum at 4 K, in units of the conductance quantum $G_0 = 2e^2/h$. The data shown begin when a high-conductivity ($n > 10$) contact had been established and then drawn down to the $n = 1$ state. The contact was then broken and reformed, then broken again. We were routinely able to hold contacts in the $n = 1$ and 2 states for ten minutes or more. There are no adjustable parameters in the experimental determination of conductance.

able to maintain the junction in the $n = 1$ or 2 state for ten minutes or more at a time, achieving the stability of MCBJ experiments with a more versatile experimental platform; we held one $n = 1$ state for > 30 min, finally breaking it deliberately to make other measurements.

Figure 5 shows an enlargement of the data from Fig. 4 over the interval $t = 750$ to 1000 s, beginning out of contact. Figure 5(a) is again the current; Fig. 5(b) shows the measured position of the probe tip relative to its starting position out of contact at $t = 750$ s, where positive tip motion corresponds to movement *toward* contact. On approach to contact, we often observed the phenomenon shown here: we began to see conduction spikes up to, but never exceeding $n \approx 0.15$. As we continued the approach, over an additional motion of 0.2 nm, the spikes became more frequent and the contact then appeared to "prefer" the $n \approx 0.15$ state, with spikes now downward toward zero conduction. At a position 0.3 nm farther inward, the system jumped to the $n = 1$ state. It stayed in the $n = 1$ state for an additional 0.7 nm motion inward, after which it jumped to a state with $n \approx 2$. The $n \approx 0.15$ state represents conduction at significantly less than G_0, yet is substantially greater than a conventional tunneling current.[36] One explanation for the phenomenon could be that there is rapid electron or atom hopping carrying charge across the gap; such an oscillation very near contact is often referred to as a two-level fluctuation.[37] Another explanation may be the effect of finite bias voltage on electron transmission through single-atom channels, as suggested by theoretical work,[38] although this would be unlikely at the low bias voltage we apply. The relatively stable state at $n \approx 0.15$ could well also be due to conduction through an impurity atom or molecule in the gap. It should be noted that the approach data in Fig. 5 were taken over several hundred seconds; the stability of the FSBJ, comparable to that of the MCBJ, allowed us to maintain each specific conduction state for extensive lengths of time and to switch between states in a controlled way, while
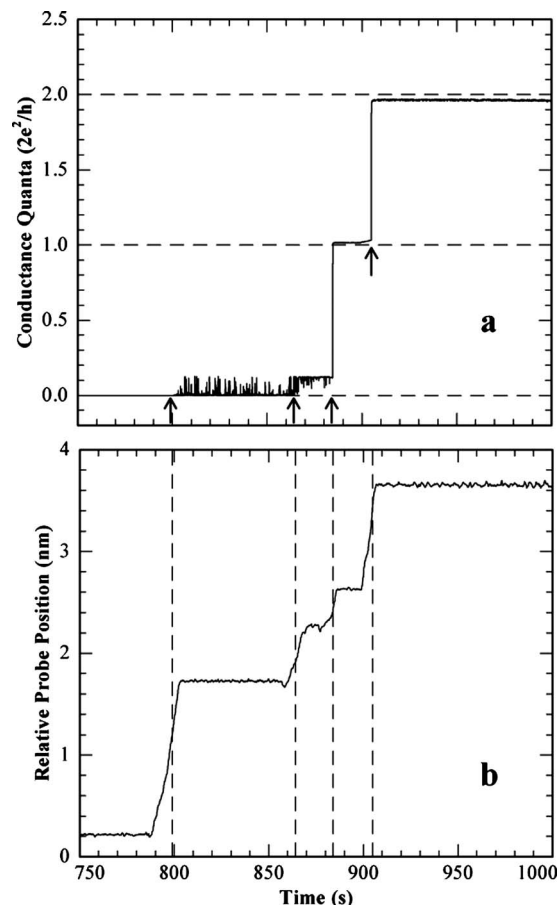

FIG. 5. (a) An enlargement of the conductance data from Fig. 4, for the time interval 750 s $< t <$ 1000 s and (b) the corresponding relative probe position, as measured interferometrically. Increasing values of relative probe position denote probe motion toward the flat. Times when conduction state transitions occurred are marked by arrows in (a) and correspond to dashed lines in (b).

simultaneously providing an accurate, direct measurement of probe position.

Figure 6 shows the effect of small changes in SAC length for a contact that is nominally in the $n \approx 1$ state, although the conductivity is slightly below $1.0 G_0$. Here, a greater number on the "relative tip extension" axis in Figs. 6(a) and 6(c) represents a probe tip position *farther* from the Au flat. That is, in Fig. 6(a), at times 14 s $< t <$ 22 s the chain is 0.6 nm shorter than at $t = 0$, whereas for times 24 s $< t <$ 32 s it is 0.6 nm longer than at $t = 0$. The interesting observation here, and one that it would not necessarily be possible to make in a less stable experimental system, is that although the entire nominal $n \approx 1$ state is stable, the conductivity of the SAC at the $t = 0$ length is, in some sense "more stable" than that seen when the SAC length is shortened or lengthened by amounts less than 1 nm. Conductivity increases when the SAC is shortened, but "noise" spikes are observed which point "back" toward the more stable value, and a reciprocal effect is seen when the chain is stretched. Figure 6(c) replots the data so as to eliminate time and clearly reveals the linear relationship between conductivity and changes in chain length, including the noise observed at the two extremes of chain length. We should emphasize here that we see this linear behavior routinely for small changes
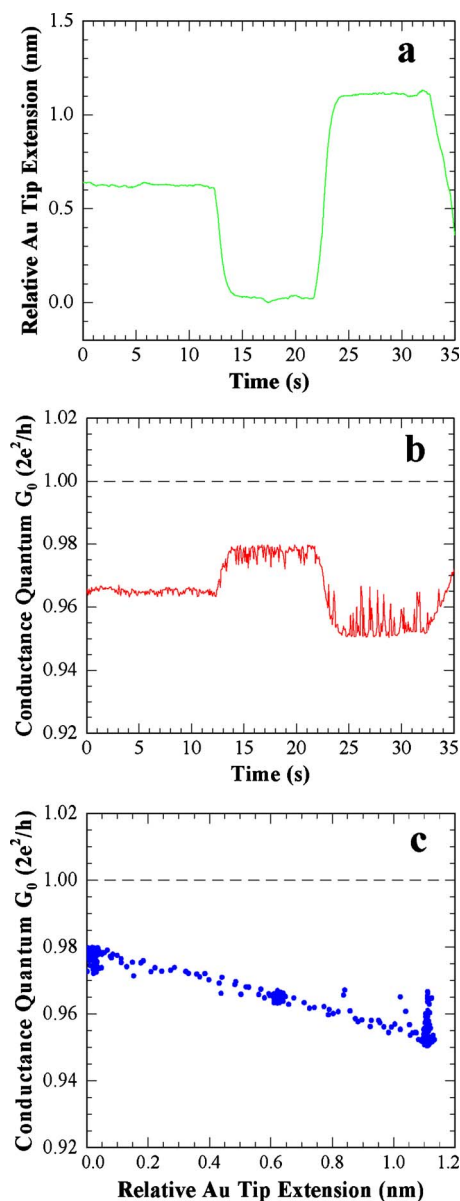
FIG. 6. (Color online) Detailed conduction behavior observed experimentally for a gold single-atom-chain near a $1G_0$ state. (a) A time trace of the change in Au tip position over a range of ≈ 1.2 nm, with increasing tip extension corresponding to an elongation of the Au chain. The data show the observed tip motion that resulted from manual changes in the servo set point. (b) The conductance, in units of G_0, for the time shown in (a). Both the average value of the conductivity and its stability are seen to vary with chain length. (c) A replotting of the data from (a) and (b) to eliminate time and show directly the relationship between chain length change and conductivity.

in SAC length, but we also routinely see discrete steps in the conductance (both increases and decreases) for greater length changes. We attribute these steps either to changes in the number of atoms in the SAC portion of the junction or to rearrangements in the structure of the supporting atoms at each end of the SAC. We are currently comparing the results of our experiments and simulations to understand these steps in detail.

The experimental observation that conductivity in the nominal $n \approx 1G_0$ state is usually slightly less than $1.0G_0$ is reasonably well understood in general terms. Quantized conduction in one-dimensional (1D) systems is in fact given not

by $G_0 = 2e^2/h$ exactly, but by $G = 2Te^2/h$, where T is the transmission coefficient. T is assumed to be identically 1 for incident electrons with zero incident energy (*i.e.*, the bias voltage across junction is zero) traversing a perfect lattice structure at zero temperature. Real experimental systems violate all three of those conditions to varying degrees; SAC conductivity measurements where the $n \approx 1$ state shows conductivity in the range $0.90G_0$ to $0.99G_0$ are the rule rather than the exception,[5,13,15] and considerable modeling work has been done to improve the understanding of inelastic effects.[39–45] Even without inelastic scattering, T can be smaller than 1 because of the wave function matching at the boundary connecting the atomic chain to wider metallic leads and within the chain itself at large elastic strains. For the behavior shown in Fig. 6, temperature and bias voltage are constant. It is therefore reasonable to suggest that the very deterministic dependence of both the average conductivity and its stochastic component on changes in SAC length is related to changes in wave function matching resulting from subtle changes in Au bond lengths and positions. The strength of the FSBJ instrument presented here is that its stability permits highly detailed studies of these transport effects.

Figure 4 also shows what appear to be several stable states with conductivity far from integer values nG_0. We show a more detailed view of such a state in Fig. 7. At $t = 0$ in Fig. 7(a), the junction had just transformed, during elongation, from a higher-conductance state ($n > 2$) into a state with conductivity $\approx 1.8G_0$. It remained stable in that state during an elongation of 0.5 nm, as shown in Fig. 7(b), before transforming to a state $n \approx 0.93G_0$, where it remained through an additional 0.4 nm of stretching before breaking.

To help understand conduction states observed experimentally (particularly those far from integer values of conductance), the atomic structures that give rise to them, and the mechanisms for transitions between the corresponding structures, we have performed DFT simulations in which initially well-ordered nanowires were semistatically elongated until rupture. As the nanowire is strained, it undergoes a series of morphological transitions, usually leading to the formation of a variety of ordered two-dimensional (2D) structures.[46] Further elongation of the wire results in the thinning of those intermediate, ordered structures into a SAC. The quantum conductance at zero bias was computed for each stage of elongation, so that a relationship between conductance behavior and structural arrangement could be determined. A typical series of structures produced in this way, with the conductance of each structure, is shown in Fig. 8. All of the DFT elongation calculations were performed using DMol (Refs. 47 and 48) with a real-space cutoff of 0.4 nm, a double-zeta, atom-centered basis set, a generalized gradient approximation approach,[49] and a hardness-conserving semilocal pseudopotential.[50] The DFT quantum conductance calculations were performed using ATK (Refs. 51 and 52) with a single-zeta, atom-centered basis set, and norm-conserving pseudopotential.[53] No inelastic scattering effects are included in the calculations.

Preliminary simulation results indicate that for nanowires with ordered 2D structures the conductance assumes
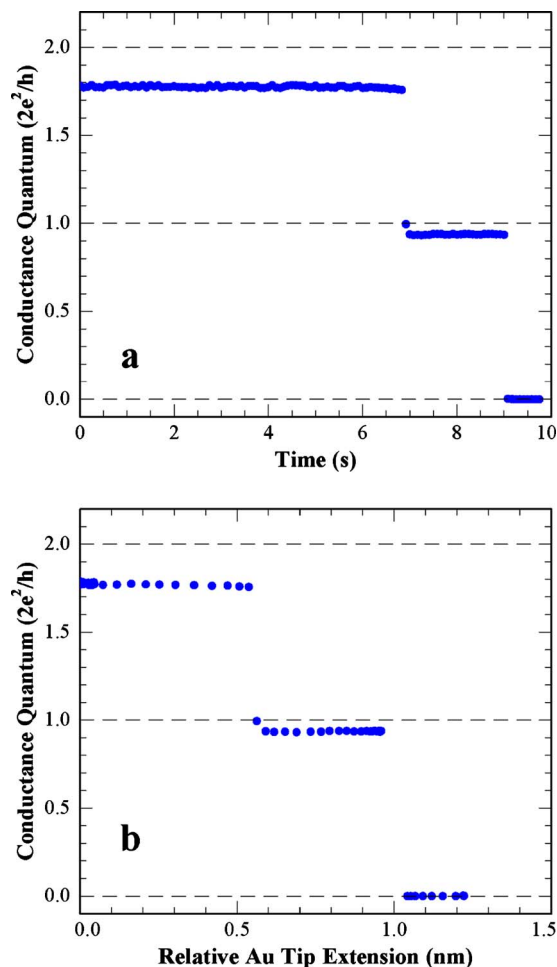
FIG. 7. (Color online) (a) A time trace of a stable conductance state observed at $\approx 1.8G_0$ which, on stretching, transitions (at $t = 6.7$ s) to a new stable state at $0.93G_0$ before breaking at $t = 9.0$ s. (b) The same data, plotted as a function of relative tip extension *away from* the flat. The $0.93G_0$ state is seen to exist for approximately 0.4 nm of chain elongation before breaking.

noninteger values of n. For example, the nanowire shown in Fig. 8 is initially in a zig-zag structure (one of the most commonly encountered intermediate structures in this work) and displays a conductance of $\approx 1.85G_0$. As the wire is elon-
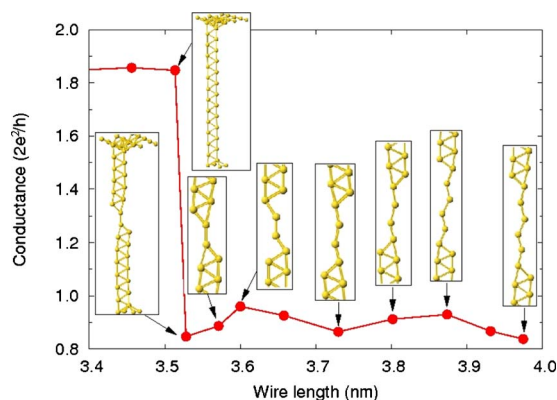

FIG. 8. (Color online) Calculated quantum conductance at zero bias vs wire length. A stable conductance state is observed near $1.85G_0$ for 2D wires with a zig-zag structure. As the wire is elongated to just beyond 3.5 nm, a two-atom SAC is formed and the conductance drops by $1G_0$. As the structure is elongated further, the SAC lengthens and the conductance oscillates around a new stable state at $0.9G_0$.

gated to just beyond 3.5 nm, a two-atom SAC is formed abruptly and the conductance immediately drops by $1G_0$. As the wire is strained further, the number of atoms belonging to the SAC increases, but the conductance remains approximately constant around $n \approx 0.9G_0$. The similarity between this simulation and the experimental results in Fig. 7 suggests that at least some of the noninteger conduction state we observe may be associated with ordered 2D structures, although there may well be other structures that show similar conductivity. Our work in relating experimentally observed conduction states and transitions to DFT simulations is ongoing.

IV. SUMMARY

We have developed an exceptionally stable experimental platform for the study of atomic-scale contacts, deformation, and electron transport properties, and have demonstrated that stability in a series of break junction experiments. By positioning an interferometer cavity directly between an Au surface and probe mount, we have significantly tightened the displacement measurement frame relative to that achieved in prior work. This allows us to close a servo loop around the junction separation with long-term, picometer stability, so as to remove thermal drift and low-frequency vibration artifacts and thereby, reduce the need for rigorous environmental isolation that is often encountered in these types of experiments. The FSBJ could greatly improve a number of contact, or near-contact, atomic-scale experiments, including fixed-separation current-voltage measurements in the tunneling regime[36] and the study of electron transport in strained SACs, as demonstrated here. The long-term stability of the nanometer-scale gap formed at a broken junction holds great promise for applications in single-molecule spectroscopy.[54,55]

In addition, our future work will incorporate a stiff elastic force sensor, so that direct mechanical measurements can be made of bond stiffness and breaking force in SACs. Our interests in this field are to establish the force associated with the rupture of a single atomic bond as an intrinsic force reference, as has been suggested by some authors,[46] and the mechanical stiffness of a single atomic bond or other stable nanowire or atomic chain structure as an intrinsic stiffness reference, with conductivity used to determine which structure is present. The interferometer design currently being used for measuring probe motion will provide sufficient sensitivity for measuring the quasistatic deflection of a stiff (100 N m^{-1}) elastic force sensor with subnanonewton precision.

Institute of Standards and Technology, nor is it intended to imply that the identified are necessarily the best available for the purpose.

[1] N. Agraït, A. L. Yeyati, and J. M. van Ruitenbeek, Phys. Rep. **377**, 81 (2003).
[2] R. Landauer, IBM J. Res. Dev. **1**, 223 (1957).
[3] M. Büttiker, Y. Imry, R. Landauer, and S. Pinhas, Phys. Rev. B **31**, 6207 (1985).
[4] M. Brandbyge, J. Schiøtz, M. R. Sørensen, P. Stoltze, K. W. Jacobsen, and J. K. Nørskov, Phys. Rev. B **52**, 8499 (1995).
[5] V. Rodrigues, T. Fuhrer, and D. Ugarte, Phys. Rev. Lett. **85**, 4124 (2000).
[6] J. L. Costa-Krämer, N. García, P. García-Mochales, P. A. Serena, M. I. Marqués, and A. Correia, Phys. Rev. B **55**, 5416 (1997).
[7] T. Frederiksen, M. Paulsson, M. Brandbyge, and A.-P. Jauho, Phys. Rev. B **75**, 205413 (2007).
[8] C. Untiedt, M. J. Caturla, M. R. Calvo, J. J. Palacios, R. C. Segers, and J. M. van Ruitenbeek, Phys. Rev. Lett. **98**, 206801 (2007).
[9] J. Moreland and J. W. Ekin, J. Appl. Phys. **58**, 3888 (1985).
[10] R. J. P. Keijsers, O. I. Shklyarevskii, J. G. H. Hermsen, and H. van Kempen, Rev. Sci. Instrum. **67**, 2863 (1996).
[11] J. Voets, R. J. P. Keijsers, O. I. Shklyarevskii, and H. van Kempen, Phys. Rev. B **53**, 1072 (1996).
[12] N. Agraït, J. G. Rodrigo, and S. Vieira, Phys. Rev. B **47**, 12345 (1993).
[13] N. Agraït, C. Untiedt, G. Rubio-Bollinger, and S. Vieira, Phys. Rev. Lett. **88**, 216803 (2002).
[14] O. Yu. Kolesnychenko, O. I. Shklyarevskii, and H. van Kempen, Rev. Sci. Instrum. **70**, 1442 (1999).
[15] G. Rubio-Bollinger, P. Joyez, and N. Agraït, Phys. Rev. Lett. **93**, 116803 (2004).
[16] A. M. C. Valkering, A. I. Mares, C. Untied, K. Babaei Gavan, T. H. Oosterkamp, and J. M. van Ruitenbeek, Rev. Sci. Instrum. **76**, 103903 (2005).
[17] K. H. Gundlach, Solid-State Electron. **9**, 949 (1966).
[18] C. Untiedt, A. I. Yanson, R. Grande, G. Rubio-Bollinger, N. Agraït, S. Vieira, and J. M. van Ruitenbeek, Phys. Rev. B **66**, 085418 (2002).
[19] N. Agraït, G. Rubio, and S. Vieira, Phys. Rev. Lett. **74**, 3995 (1995).
[20] G. Rubio, N. Agraït, and S. Vieira, Phys. Rev. Lett. **76**, 2302 (1996).
[21] G. Rubio-Bollinger, S. R. Bahn, N. Agraït, K. W. Jacobsen, and S. Vieira, Phys. Rev. Lett. **87**, 026101 (2001).
[22] S. P. Jarvis, M. A. Lantz, H. Ogiso, H. Tokumoto, and U. Dürig, Appl. Phys. Lett. **75**, 3132 (1999).
[23] P. E. Marszalek, W. J. Greenleaf, H. Li, A. F. Oberhauser, and J. M. Fernandez, Proc. Natl. Acad. Sci. U.S.A. **97**, 6282 (2000).
[24] A. W. Sparks and S. R. Manalis, Nanotechnology **17**, 1574 (2006).
[25] H. Ohnishi, Y. Kondo, and K. Takayanagi, Nature (London) **395**, 780 (1998).
[26] T. Kizuka, S. Umehara, and S. Fujisawa, Jpn. J. Appl. Phys., Part 2 **40**, L71 (2001).
[27] T. Kizuka, Phys. Rev. B **77**, 155401 (2008).
[28] E. Z. da Silva, A. J. R. da Silva, and A. Fazzio, Comput. Mater. Sci. **30**, 73 (2004).
[29] H. S. Park, K. Gall, and J. A. Zimmerman, J. Mech. Phys. Solids **54**, 1862 (2006).
[30] N. V. Skorodumova, S. I. Simak, A. E. Kochetov, and B. Johansson, Phys. Rev. B **75**, 235440 (2007).
[31] F. Sato, A. S. Moreira, P. Z. Coura, S. O. Dantas, S. B. Legoas, D. Ugarte, and D. Galvao, Appl. Phys. A: Mater. Sci. Process. **81**, 1527 (2005).
[32] Attocube ANPx50 and ANPx51, attocube systems AG, Munich, Germany.
[33] M. L. Trouwburst, E. H. Huisman, F. L. Bakker, S. J. van der Molen, and B. J. van Wees, Phys. Rev. Lett. **100**, 175502 (2008).
[34] D. T. Smith, J. R. Pratt, and L. P. Howard, Rev. Sci. Instrum. **80**, 035105 (2009).
[35] S. L. Gilbert, W. C. Swann, and C.-M. Wang, NIST Special Publication 260–137, 2005 Edition.
[36] J. A. Strosio and W. J. Kaiser, *Scanning Tunneling Microscopy*, Methods of Experimental Physics Vol. 27 (Academic, New York, 1993).
[37] C. J. Muller, J. M. van Ruitenbeek, and L. J. de Jongh, Phys. Rev. Lett. **69**, 140 (1992).
[38] M. Brandbyge, N. Kobayashi, and M. Tsukada, Phys. Rev. B **60**, 17064 (1999).
[39] T. Frederiksen, M. Brandbyge, N. Lorente, and A.-P. Jauho, Phys. Rev. Lett. **93**, 256601 (2004).
[40] Y. J. Lee, M. Brandbyge, M. J. Puska, J. Taylor, K. Stokbro, and R. M. Nieminen, Phys. Rev. B **69**, 125409 (2004).
[41] M. Paulsson, T. Frederiksen, and M. Brandbyge, Phys. Rev. B **72**, 201101 (2005).
[42] J. K. Viljas, J. C. Cuevas, F. Pauly, and M. Häfner, Phys. Rev. B **72**, 245415 (2005).
[43] N. V. Skorodumova, S. I. Simak, A. E. Kochetov, and B. Johansson, Phys. Rev. B **72**, 193413 (2005).
[44] A. Grigoriev, N. V. Skorodumova, S. I. Simak, G. Wendin, B. Johansson, and R. Ahuja, Phys. Rev. Lett. **97**, 236807 (2006).
[45] H. Nakamura, J. Phys.: Condens. Matter **20**, 224023 (2008).
[46] F. Tavazza, L. E. Levine, and A. M. Chaka, J. Appl. Phys. **106**, 043522 (2009).
[47] B. Delley, J. Chem. Phys. **92**, 508 (1990).
[48] B. Delley, J. Chem. Phys. **113**, 7756 (2000).
[49] J. P. Perdew, K. Burke, and M. Ernzerhof, Phys. Rev. Lett. **77**, 3865 (1996).
[50] B. Delley, Phys. Rev. B **66**, 155125 (2002).
[51] Atomistix ToolKit version x.x, QuantumWise A/S, www.quantumwise.com.
[52] M. Brandbyge, J.-L. Mozos, P. Ordejón, J. Taylor, and K. Stokbro, Phys. Rev. B **65**, 165401 (2002).
[53] M. Soler, E. Artacho, J. D. Gale, A. García, J. Junquera, P. Ordejón, and D. Sánchez-Portal, J. Phys.: Condens. Matter **14**, 2745 (2002).
[54] A. Nitzan and M. A. Ratner, Science **300**, 1384 (2003).
[55] Z. Qian, R. Li, S. Hou, Z. Xue, and S. Sanvito, J. Chem. Phys. **127**, 194710 (2007).